Reactions of the $[Fe(CN)_5NO]^{2-}$ complex with biologically relevant thiols

Konrad Szaciłowski,[a] Alicja Wanat,[a] Andrea Barbieri,[b] Ewa Wasielewska,[a] Małgorzata Witko,[c] Grażyna Stochel[a] and Zofia Stasicka*[a]

[a] *Faculty of Chemistry, Jagiellonian University, Ingardena 3, 30-060, Kraków, Poland*
[b] *Department of Chemistry, University of Ferrara, Via Borsari 46, 44100, Ferrara, Italy*
[c] *Institute of Catalysis and Surface Chemistry, Polish Academy of Sciences, Niezapominajek 6, 30-239, Kraków, Poland*

Received (in Strasbourg, France) 14th May 2002, Accepted 10th July 2002
First published as an Advance Article on the web 16th September 2002

Reactions of the $[Fe(CN)_5NO]^{2-}$ complex with biologically relevant thiols (H_nRS = cysteine, *N*-acetylcysteine, ethyl cysteinate and glutathione) are initiated by the nucleophilic attack of a thiolate (RS^{n-}) on the N atom of the NO^+ ligand in the complex to form $[Fe(CN)_5N(O)SR]^{(n+2)-}$. The N–S bond in the latter complex is, however, weak and can undergo both heterolytic and homolytic splitting. The former process makes the synthesis reaction reversible, whereas the latter is responsible for the spontaneous redox decomposition: $[Fe(CN)_5N(O)SR]^{(n+2)-} \rightarrow [Fe^{II}(CN)_5NO]^{3-} + RS^{\bullet(n-1)-}$. The rate of the monomolecular reaction is controlled by an inductive effect in the thiol with an additional stabilisation coming from formation of a six-membered ring in the case of the *N*-acylated compounds. In the presence of thiolate excess, the $RS^{\bullet(n-1)-}$ radicals are transformed into the more stable $RSSR^{\bullet(2n-1)-}$ radicals, which are scavenged by both $[Fe(CN)_5N(O)SR]^{(n+2)-}$ and $[Fe(CN)_5NO]^{2-}$. The former reaction initiates, whereas the latter terminates, chain reactions of the catalysed redox decomposition. The catalytic decomposition (in the thiol excess) is much faster than the spontaneous decay (in the nitroprusside excess) but leads to the same final products. The Fe(II) reduction product is identified by UV/Vis, IR, electrochemical and EPR methods. The effect of molecular oxygen is investigated and explained. The mechanism is interpreted in terms of intermediate $[Fe(CN)_5N(O)(SR)_2]^{(2n+2)-}$ complex formation *via* nucleophilic attack and its decay mainly *via* homolytic splitting of the N–S bond. To verify the mechanism, a simple reaction model is constructed, based on the assumption that the $RSNO^{(n-1)-}$ ligands are mostly responsible for the $[Fe(CN)_5N(O)(SR)]^{(n+2)-}$ reactivity and their electronic properties are discussed within the DFT framework.

Nitric oxide is a potent vasorelaxant and neurotransmitter and therefore NO delivery to selected biological targets is of great importance.[1–10] Different organic and inorganic NO donors are currently applied, among them sodium pentacyanonitrosylferrate (customarily named sodium nitroprusside), which is the only clinically used metal nitrosyl complex.[11] It is used as a hypotensive anaesthetic during surgery and in the treatment of erythromelalgia. It is known to induce a very rapid physiological response, which becomes evident within seconds after the infusion. Its metabolism is quite different from other common NO donors (like nitroglycerine, syndonimines, *S*-nitrosothiols or NONOates).[12,13] Nitroprusside can react with numerous compounds present in mammalian cells, but most of these processes are far too slow. The only known process fast enough to be responsible for such an effect is the reaction between the $[Fe(CN)_5NO]^{2-}$ complex and a thiolate anion.[14–16] Several components of cellular medium contain thiol groups; the most important are cysteine, homocysteine and glutathione. The mechanism of this physiological activity is still not elucidated, although the reactions between nitroprusside and thiolates have been studied extensively.[14–27] It is believed, however, that reduction of nitroprusside is the first stage of its metabolism with subsequent contribution of membrane-bound enzymes.

It is well evidenced that nitroprusside in the presence of a thiolate anion is transformed into the *S*-nitrosothiolato-*N* complex *via* a nucleophilic attack on the NO ligand:[14–27]

$$[Fe(CN)_5NO]^{2-} + RS^{n-} \rightleftharpoons [Fe(CN)_5N(O)SR]^{(n+2)-}, \quad K_1 = k_1/k_{-1} \qquad (1)$$

The nitrosothiol complexes, $[Fe(CN)_5N(O)SR]^{(n+2)-}$, are generated immediately upon mixing solutions containing nitroprusside and a thiol. The reaction is accompanied by a colour change from yellow to purple-red {all as yet known $[Fe(CN)_5N(O)SR]^{(n+2)-}$ complexes are characterised by λ_{max} = 522–526 nm, $\varepsilon_{max} \sim 10^3$–$10^4$ M^{-1} cm^{-1}}.[16] In almost all studied cases a fast decomposition is the next step, which is accompanied with bleaching of the reaction mixture to a yellowish brown colour and formation of a Fe(II) complex and disulfide as the ultimate products.[15,16,18,21–23]

The structure of the thiolate anion was found to influence the $[Fe(CN)_5N(O)SR]^{(n+2)-}$ stability: the presence of electron-withdrawing groups stabilises, while electron-rich groups destabilise the complex.[16] The rate of the redox decomposition depends also on other factors, such as the nitroprusside to thiol ratio and the presence of molecular oxygen. The decomposition of the $[Fe(CN)_5N(O)SR]^{4-}$ complex (H_2RS = cysteine) was reported to occur spontaneously both in the presence of an excess of nitroprusside and cysteine; in the latter case the reaction was much faster that in the former case.[21,22] Moreover, the presence of oxygen was found to increase the

stability of the coloured species.[21] The role of these parameters is not yet cleared up and even identification of the final product is questionable: in some papers formation of the $[Fe(CN)_5NO]^{3-}$ complex is reported,[16,21,22] while in others the $[Fe(CN)_4NO]^{2-}$ species is claimed to be the final product.[15,18,19]

Thus, despite numerous studies,[14–27] the mechanism of the $[Fe(CN)_5N(O)SR]^{(n+2)-}$ decomposition is not fully understood. In this paper, we present a detailed analysis of the complex product and kinetics of the decomposition of the $[Fe(CN)_5N(O)SR]^{(n+2)-}$ complexes with two biologically relevant thiols: cysteine and glutathione; to follow the effect of the thiol structure—two cysteine derivatives (ethyl cysteinate, *N*-acetylcysteine) are also included. In order to interpret the kinetic results, the reactions are modelled using DFT calculations.

Results and discussion

Product analysis

Reduction of nitroprusside, both chemical and electrochemical, may lead to direct formation of two different reaction products. In acidic media or in non-aqueous solutions the blue $[Fe(CN)_4NO]^{2-}$ complex is the main product, while in alkaline media the brown $[Fe(CN)_5NO]^{3-}$ ion is generated. Changes in pH and cyanide concentration induce an interconversion of the complexes:[27–31]

$$[Fe(CN)_5NO]^{3-} \underset{OH^-,CN^-}{\overset{H^+}{\rightleftharpoons}} [Fe(CN)_4NO]^{2-} \qquad (2)$$

Ascorbic acid in acidic solution reduces nitroprusside to $[Fe(CN)_4NO]^{2-}$, whereas in alkaline solution the $[Fe(CN)_5NO]^{3-}$ complex is formed.[29,32,33] The reaction between nitroprusside and thiols such as cysteine, ethyl cysteinate, *N*-acetylcysteine and glutathione needs alkaline medium to proceed. Under these conditions, an initial increase in absorption characteristic of $[Fe(CN)_5N(O)SR]^{(n+2)-}$, is followed by its decrease and growth of two new bands with λ_{max} at 350 and 440 (sh) nm. The band assignment to $[Fe(CN)_5NO]^{3-}$ [29,30,34] is supported by the spectroelectrochemical measurements. Reduction of nitroprusside at a platinum minigrid electrode at −0.5 V *vs.* Ag/AgCl at pH 10 yields an air sensitive species that is characterised by the two absorption bands at 350 and 440 nm, whose properties can only be attributed to $[Fe(CN)_5NO]^{3-}$ [30–33,35,36]. The assignment is confirmed by IR as well as ESR experiments.

IR detection shows that the reaction between nitroprusside and a thiolate is accompanied by immediate formation of two intense peaks at 2100 and 2074 cm^{-1} {assigned to ν_{CN} in the $[Fe(CN)_5N(O)SR]^{(n+2)-}$ complex.}[16,34] In the next step, these bands decay gradually and a new peak at 2088 cm^{-1} is formed. The latter value is consistent with the 2088–2090 cm^{-1} reported as characteristic of the $[Fe(CN)_5NO]^{3-}$ complex.[34,37]

EPR investigations of the nitroprusside–thiolate system made at room temperature (Fig. 1) revealed the generation of only one stable paramagnetic species, whose spectral parameters: $g = 2.027$, $a(N) = 14.0$ G, are close to those reported for $[Fe(CN)_5NO]^{3-}$ [$g = 2.027$, $a(N) = 14.8$ G].[38–41] This observation is consistent with previous reports.[16,21,22,36] However, at lower pH or in the case of certain thiols[16] formation of the $[Fe(CN)_4NO]^{2-}$ complex and release of cyanide cannot be excluded.[15,16,18,19,37,39]

All these results unambiguously confirm the earlier presumptions[14] that the thermal decomposition of $[Fe(CN)_5N(O)SR]^{(n+2)-}$ (RS^{n-} = anions of cysteine, ethyl cysteinate, *N*-acetylcysteine or glutathione) leads to the generation of the $[Fe(CN)_5NO]^{3-}$ complex. Moreover, the results show that neither detectable amounts of $[Fe(CN)_4NO]^{2-}$, nor other paramagnetic Fe complexes, are formed from nitroprusside under these conditions.

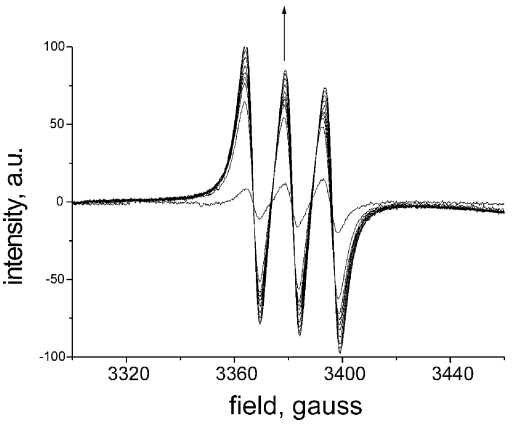

Fig. 1 EPR spectra of the oxygen-free system consisting of 0.1 M $[Fe(CN)_5NO]^{2-}$ and 0.1 M cysteine at pH = 10, $T = 298$ K; the spectra were measured immediately after mixing the reagents (the lowest spectrum recorded) and every 60 s; the signal recorded at $g = 2.027$, $a(N) = 14.0$ G is characteristic of the $[Fe(CN)_5NO]^{3-}$ product.

Kinetics

Nitroprusside excess. At high nitroprusside excess (10- to 200-fold), decomposition of the $[Fe(CN)_5N(O)SR]^{(n+2)-}$ complex proceeds according to first-order kinetics, with k_{obs} independent of nitroprusside concentration. Thus, the reaction can be considered as the reversible homolytic splitting of the N–S bond, accompanied by generation of the $RS^{\bullet(n-1)-}$ radicals, which are the source of disulfides:

$$[Fe(CN)_5N(O)SR]^{(n+2)-} \rightleftharpoons [Fe(CN)_5NO]^{3-} + RS^{\bullet(n-1)-}, \quad k_3/k_{-3} \qquad (3)$$

The kinetics are consistent with an empirical kinetic equation for a system with a pre-equilibrium:[42]

$$k_{obs}^{NP} = \frac{K_1 k_3 [NP]}{1 + K_1 [NP]} + k_{-3} \qquad (4)$$

where NP denotes nitroprusside, K_1 is the pre-equilibrium [eqn. (1)] constant, whereas k_3 and k_{-3} are the rate constants of the inner-sphere redox decomposition [eqn. (3)]. As K_1 values are relatively large (see Table 1), at high NP concentration the relation (4) is simplified to $k_{obs}^{NP} = k_3 + k_{-3}$. The lack of effect of the NP concentration under the studied conditions indicates that the concentration used is high enough to reach the limiting value of k_{obs}^{NP}.

The rates of the monomolecular (inner-sphere) redox decomposition ($k_3 + k_{-3}$ values in Table 1) depend on the thiol structure, which correlates well with the inductive effect.[16] The presence of the $-NH_2$ group destabilises, whereas the carboxylic group stabilises, the $[Fe(CN)_5N(O)SR]^{(n+2)-}$ complex. However, when the groups are blocked by acetylation or esterification for example, their influence is suppressed.[16] Thus, the presence of unprotected COO^- and acetylated amino groups makes the complex with *N*-acetylcysteine the most stable in the series. In contrast, the complex with ethyl cysteinate having unprotected $-NH_2$ and protected $-COO^-$ groups undergoes the fastest decomposition. The effect of both unprotected groups is similar to that where both groups are blocked, giving virtually no difference in the reaction rates between glutathione and cysteine complexes. The formation of a six-membered ring by *N*-acylated thiols[43] results in a strengthening of the S–N bond at the expense of the N–O bond (Scheme 1). This effect may contribute also to the increased stability (the lowest

Table 1 Rate constants of spontaneous ($k_3 + k_{-3}$) and catalytic reduction (k_0, k_I) of the $[Fe(CN)_5N(O)SR]^{(n+2)-}$ complexes by selected thiols, collated with the constants (K_1) of the equilibrium reaction 1 and the ionisation constants (pK_a) of the parent thiols, H_nSR ($T = 298$ K, $[Na^+] = 0.66$ M)

Thiolate	q_T[a]	pK_a[14]	K_1	$(k_3+k_{-3})/s^{-1}$	k_0[b] $/Ms^{-1}$	k_I[c] $/s^{-1}$
N-Acetylcysteine	−2	9.52	220	0.0014 ± 0.0001	0.0043 ± 0.0001	0.059 ± 0.001
Ethyl cysteinate	−1	6.5	190	0.0037 ± 0.0001	0.012 ± 0.001	0.164 ± 0.008
Cysteine	−2	8.3	210	0.0021 ± 0.0001	0.017 ± 0.001	0.210 ± 0.02
Glutathione	−3	8.75	95	0.0020 ± 0.0001	0.0035 ± 0.0001	0.129 ± 0.02[b]

[a] Total charge of the entity. [b] Calculated for high excess (120–200) of thiolate. [c] Calculated according to eqn. (12) except for glutathione, for which eqn. (13) was used.

$k_3 + k_{-3}$ values) in the case of *N*-acetylcysteine and glutathione complexes. Moreover, the strength of the S–N bond in the $[Fe(CN)_5N(O)SR]^{(n+2)-}$ complex correlates well with the strength of the S–H bond in thiols. The higher the pK_a value of the thiol dissociation, the less probable is spontaneous decomposition of the $[Fe(CN)_5N(O)SR]^{(n+2)-}$ complex (*cf.* Table 1).

The influence of oxygen on the nature of the final products in this case is negligible. Although under aerobic conditions the $[Fe(CN)_5NO]^{3-}$ complex can be reoxidised to $[Fe(CN)_5NO]^{2-}$,[25] in alkaline medium, however, the reaction is relatively slow and the reoxidation of $[Fe(CN)_5NO]^{3-}$ and any significant regeneration of $[Fe(CN)_5N(O)SR]^{(n+2)-}$ is not observed, unless an additional thiolate is present.[16] The only difference consists in the fate of the $RS^{\bullet(n-1)-}$ radicals, which are scavenged by O_2 (*vide infra*).

Thiolate excess. At high concentration of the thiolate (10- to 200-fold excess), the reduction of iron proceeds much faster than it does at the nitroprusside excess. Under these conditions, kinetic traces depend strongly on the presence of oxygen, but even those recorded under anaerobic pseudo-first-order conditions cannot be simply approximated by mono-exponential curves. Instead, the traces are indicative of autocatalysis: they start from an induction period, followed by pseudo-zero-order and, at the end, by pseudo-first-order fragments of the curve (Fig. 2).

Analysis of the induction period shows that catalyst formation is accelerated by an increased RS^{n-} concentration and decelerated by an increased concentration of molecular oxygen. The initial increase in the reaction rate depends additionally on the thiolate nature and under the same conditions follows the series:

$$\text{cysteine} > \text{ethyl cysteinate} > \text{glutathione} > \textit{N}\text{-acetylocysteine} \quad (5)$$

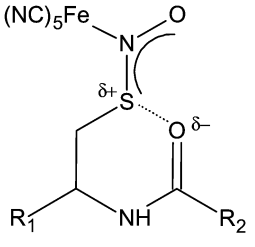

S-nitroso-*N*-acetylcysteine:

$R_1 = COO^-$, $R_2 = CH_3$

S-nitrosoglutathione:

$R_1 = CONHCH_2COO^-$, $R_2 = CH_2CH_2CH(NH_2)COO^-$

Scheme 1 Model of intramolecular stabilisation of the N–S bond due to formation of the six-membered rings in the $[Fe(CN)_5N(O)SR]^{(n+2)-}$ complexes with the *N*-acylated *S*-nitrosothiols (*N*-acetylcysteine and glutathione) (adapted from ref. 40).

The chain reaction is initiated by the $RS^{\bullet(n-1)-}$ radicals, produced originally in the spontaneous redox decomposition of $[Fe(CN)_5N(O)SR]^{(n+2)-}$ [eqn. (3)], which are scavenged by the thiolate ions and transformed into the $RSSR^{\bullet(2n-1)-}$ radicals:[44–46]

$$RS^{\bullet(n-1)-} + RS^{n-} \rightleftharpoons RSSR^{\bullet(2n-1)-}, \quad k_6/k_{-6} \quad (6)$$

This reaction proceeds somewhat faster in the case of cysteine than glutathione radicals ($k_6 = 1.2 \times 10^9$ and $4.5–5.8 \times 10^8$ $dm^3\ mol^{-1}\ s^{-1}$ for cysteine and glutation, respectively)[47–49] and O_2 scavenger competes effectively with thiolates (*vide infra*). These effects are consistent with the differences in the induction period duration.

The $RSSR^{\bullet(2n-1)-}$ radicals, known from their reducing and nucleophilic properties,[44–51] can be scavenged by both complexes involved in the equilibrium (1): The reaction with $[Fe(CN)_5N(O)SR]^{(n+2)-}$ should be responsible for chain propagation, whereas that with $[Fe(CN)_5NO]^{2-}$ for the chain termination. The former can proceed if the dithiolato transient species can be formed as a result of the nucleophilic attack of the dithiolate radical on the O–N–S fragment of the $[Fe(CN)_5N(O)SR]^{(n+2)-}$ complex:

$$[Fe(CN)_5N(O)SR]^{(n+2)-} + RSSR^{\bullet(2n-1)-} \rightleftharpoons [Fe(CN)_5N(O)(SR)_2]^{(2n+2)-} + RS^{\bullet(n-1)-} \quad (7)$$

This reaction resembles the nucleophilic attack of thiolate anion on the nitrogen atom of the nitrosothiol, which can be followed by successive processes leading to oxidation of sulfur at the expense of the NO reduction.[43,52–60] In the case of the nitrosothiol bound to the Fe atom, the electron would be transferred through NO to the central atom, yielding the Fe(I) complex:

$$[Fe(CN)_5N(O)(SR)_2]^{(2n+2)-} \rightleftharpoons [Fe(CN)_5NO]^{3-} + RSSR^{\bullet(2n-1)-} \quad (8)$$

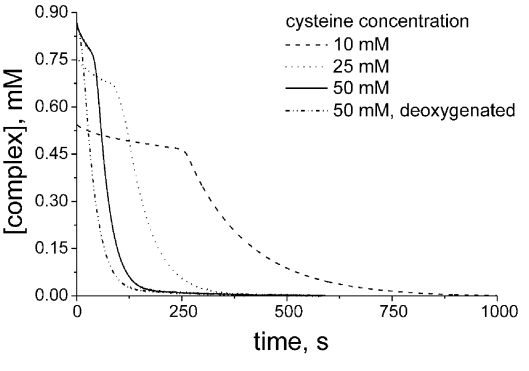

Fig. 2 Effect of cysteine concentration on the decay rate of the $[Fe(CN)_5N(O)SR]^{(n+2)-}$ complex at 1 mM total Fe concentration, pH = 10 and $T = 298$ K, as recorded at $\lambda = 600$ nm in aerated ($[O_2] \approx 0.1$ mM) and deaerated solutions.

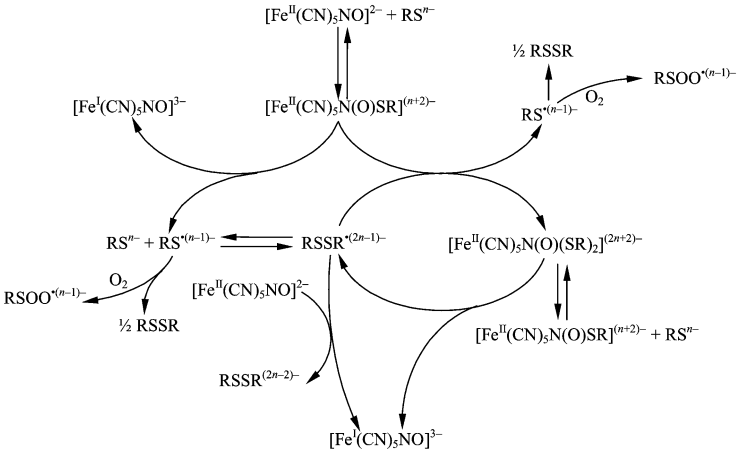

Scheme 2 Spontaneous homolytic splitting of the $[Fe(CN)_5N(O)SR]^{(n+2)-}$ complex followed by autocatalytic redox reactions proceeding at the thiolate excess. The molecular oxygen contribution is also included.

The sequence of reactions [eqns. (6)–(8)] not only reproduces but also generates additional amounts of the $RSSR^{\bullet(2n-1)-}$ radicals and therefore is responsible for the chain mechanism of the $RSSR^{\bullet(2n-1)-}$ catalysed redox decomposition of the $[Fe(CN)_5N(O)SR]^{(n+2)-}$ complex (Scheme 2).

The reaction between $[Fe(CN)_5NO]^{2-}$ and $RSSR^{\bullet(2n-1)-}$ terminates the chain mechanism due to radical consumption and generation of the final products:

$$[Fe(CN)_5NO]^{2-} + RSSR^{\bullet(2n-1)-} \overset{(2n-2)H^+}{\rightleftharpoons} [Fe(CN)_5NO]^{3-} + RSSR \quad (9)$$

Recombination of the $RS^{\bullet(n-1)-}$ radicals:

$$RS^{\bullet(n-1)-} + RS^{\bullet(n-1)-} \overset{(2n-2)H^+}{\rightleftharpoons} RSSR \quad (10)$$

as well the heterolytic decomposition of the intermediate $[Fe(CN)_5N(O)(SR)_2]^{(2n+2)-}$:

$$[Fe(CN)_5N(O)(SR)_2]^{(2n+2)-} \rightleftharpoons [Fe(CN)_5N(O)SR]^{(n+2)-} + RS^{n-} \quad (11)$$

can contribute to the termination of the catalytic cycle.

As long as the production of the $RSSR^{\bullet(2n-1)-}$ radicals compensates for their consumption the pseudo-zero-order kinetics in $[Fe(CN)_5N(O)SR]^{(n+2)-}$ concentration is observed. This means that the intermediate steps [eqns. (6) and (7)] are very fast, whereas decomposition of the transient $[Fe(CN)_5N(O)(SR)_2]^{(2n+2)-}$ species [eqn. (8)] is the rate-determining step. Pseudo-zero-order kinetics plays a more important role at large thiol excess and depends on the thiol nature mostly according to the thiolate reactivity series [eqn. (5), k_0 in Table 1].

However, as the reaction proceeds, the concentration of $[Fe(CN)_5N(O)(SR)_2]^{(2n+2)-}$ decreases and the first-order pathway starts to contribute substantially to the rate of the overall process. The pseudo-first-order behaviour is observed earlier at lower excess of thiolates. Analysis of the first-order k_{obs} dependence on the thiolate concentration (Fig. 3) shows that for cysteine, ethyl cysteinate and *N*-acetylcysteinate the kinetics is again consistent with an empirical kinetic equation [eqn. (12)] for a system with a pre-equilibrium [eqn. (1)]:

$$k_{obs}^{RS} = \frac{K_1 k_I [RS^{n-}]}{1 + K_1 [RS^{n-}]} \quad (12)$$

where k_I is the pseudo-first-order rate constant. Only in the case of glutathione is a better fit of the experimental data obtained with eqn. (13); this indicates substantial contribution of another process involving the thiolate anion.

$$k_{obs}^{RS} = \frac{K_1 k_1 [RS^{n-}]^2}{1 + K_1 [RS^{n-}]^2} \quad (13)$$

To interpret this dependence, formation of the transient dithiolate complex in the competitive reaction between $[Fe(CN)_5N(O)SR]^{(n+2)-}$ and the thiolate anion [reverse of eqn. (11)] is considered. The slower scavenging of the $RS^{\bullet(n-1)-}$ radicals, the tendency of these radicals to be converted into the C-centred isomers[61–63] and the strong reducing properties of glutathione[64,65] advocate this hypothesis.

The crucial role of the $RSSR^{\bullet(2n-1)-}$ radicals in activation of the $[Fe(CN)_5N(O)SR]^{(n+2)-}$ decay is confirmed by the kinetic traces recorded in the presence of oxygen. In this case, the induction period is much longer than in deaerated solutions (Fig. 2). The break in the kinetic curve correlates well with the time of complete oxygen consumption (Fig. 4). The duration of the first period depends not only on the O_2 but also on the thiolate concentration and nature, consistent with the thiolate reactivity series [eqn. (5)]. The increased

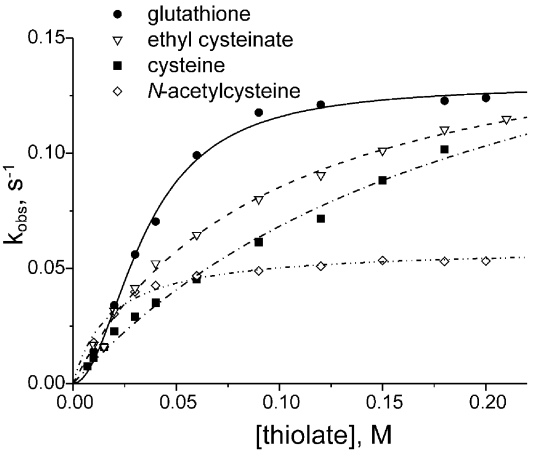

Fig. 3 Effect of thiol concentration on k_{obs} of the pseudo-first order decay of $[Fe(CN)_5N(O)SR]^{(n+2)-}$ calculated according to eqn. (12) for ethyl cysteinate, cysteine and *N*-acetylcysteine, and according to eqn. (13) for glutathione. Experimental conditions: total Fe concentration 1 mM, pH = 10, T = 298 K.

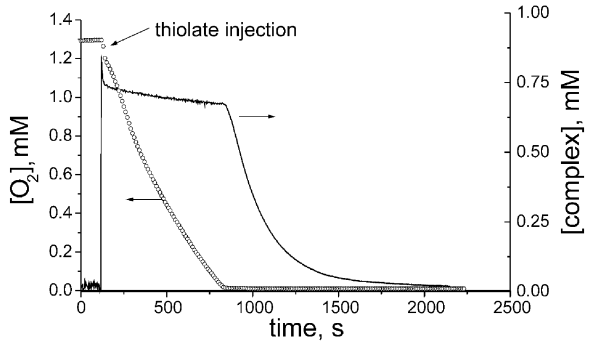

Fig. 4 Correlation between oxygen concentration and shape of the kinetic curve, recorded as change in absorption of $[Fe(CN)_5N(O)SR]^{(n+2)-}$ (RS^{n-} = 2-mercaptopropionate) at 650 nm (right scale); total Fe concentration and initial concentration of thiolate are 1 mM and 50 mM, respectively, $T = 298$ K, pH 10, buffer was saturated with molecular oxygen prior to the measurement.

oxygen concentration prolongs, whereas the increased thiolate concentration shortens the induction period (Fig. 2).

This behaviour may be interpreted in terms of competition between the two scavengers of the $RS^{\bullet(n-1)-}$ radicals [eqns. (6) and (14)]:

$$RS^{\bullet(n-1)-} + O_2 \rightarrow RSOO^{\bullet(n-1)-} \rightarrow RSO^{\bullet} + [O], \quad k_{14} \quad (14)$$

The rate of the $RS^{\bullet(n-1)-}$ scavenging by O_2 is similar to that by cysteine ($k_{14} = 1.6 \times 10^9$ M^{-1} s^{-1}), whereas in the case of glutathione it is about 10 times greater than k_6 ($k_{14} = 8.0 \times 10^9$ M^{-1} s^{-1}).[50–52] Consistent with the differences in the rate constants, the induction periods for glutathione are much longer than for cysteine. When oxygen is exhausted, the thiolate becomes the only scavenger, generation the $RSSR^{\bullet(2n-1)-}$ radicals is enhanced and the chain mechanism [eqns. (7)–(9)] is initiated and proceeds as in a deoxygenated system (Scheme 2).

To recapitulate, the pathway of the $[Fe(CN)_5N(O)SR]^{(n+2)-}$ decay consists in its redox decomposition yielding the Fe(II) complex and the $RS^{\bullet(n-1)-}$ radical, in spontaneous [eqn. (3)] or, under the RS^{n-} excess, in a process catalysed by the $RSSR^{\bullet(2n-1)-}$ radicals [eqns. (6)–(8)]. The conversion of these radicals into disulfides [eqn. (9)] is the chain termination step. As the radical mechanism presented above involves the transient dithiolato complex, whose existence could not be confirmed experimentally, DFT calculations were used to substantiate the proposal.

Modelling

To interpret the reactions of spontaneous and catalysed decomposition of $[Fe(CN)_5N(O)SR]^{(n+2)-}$, a simple reaction model was constructed, based on the assumption that it is the $RSNO^{(n-1)-}$ ligand that is mostly responsible for the reactivity. In this approach the rest of the complex is ignored and its interaction is mimicked to some extent by protonation of the N atom of the $RSNO^{(n-1)-}$ group.

Such a procedure is supported by the low stability of nitrosothiols (much lower than that of their parent thiols) and their propensity to react with thiolates and thiols.[43,52–60] The reactions with thiolates are initiated by the nucleophilic attack of the thiolate on the NO group of an *S*-nitrosothiol followed by the homo- or heterolytic splitting of the S–N bond. In consequence, the nitrosyl group transfers from one thiol moiety to another in a so-called transnitrosation process. Reactions of *S*-nitrosothiols with thiols generally consist of a 1,2-addition reaction at the N=O bond, followed by the homo- or heterolytic splitting of the S–N bond. Consequently, the nitrosyl group is transferred or the sulfur moiety is oxidised at the expense of the NO group reduction.[43,52–60]

The behaviour of the $RSNO^{(n-1)-}$ ligand in the $[Fe(CN)_5N(O)SR]^{(n+2)-}$ complex is found to resemble that of its parent nitrosothiol in undergoing both heterolytic and homolytic splittings of the S–N bond: the former is accompanied with the formation of $[Fe(CN)_5NO]^{2-}$ and RS^{n-} ions, that is the inverse reaction of complex synthesis [eqn. (1)], whereas the homolytic splitting leads to the formation of $[Fe(CN)_5NO]^{3-}$ and $RS^{\bullet(n-1)-}$ species, that is the products of the redox decomposition [eqn. (3)].

In order to model the reaction, the electronic properties of $RSNO^{(n-1)-}$ ligands (H_nRS = cysteine, *N*-acetylcysteine, ethyl cysteinate and glutathione) are discussed within the DFT framework.[66] The results of the calculations confirm the expected nucleophilic properties of the studied thiols (Table 2). In all cases the HOMO orbital is localised mostly (~90%) on the sulfur atom (see Fig. 5), which is negatively charged (−0.65 on average).

Moreover, the DFT calculations indicate that a successive addition of NO^+ and H^+ to the thiolate results in a considerable decrease in the energy difference between the frontier orbitals (HOMO – LUMO) (*cf.* Tables 2–4). According to Pearson's hardness definition,[67,68] this means that the ligand hardness decreases, whereas its polarizability increases, in the series

$$RS^{n-} > RSNO^{(n-1)-} > RSNOH^{(n-2)-} \quad (15)$$

The lowered barrier between the HOMO and LUMO orbitals may influence the LUMO population, and, consequently, may lead to a decrease of the compound stability. This would explain the decreased stability of nitrosothiolates and nitrosothiols in comparison with their parent thiolates and thiols, respectively.

Propensity of the $RSNO^{(n-1)-}$ group to undergo nucleophilic attack is also confirmed by the character of the frontiers orbitals of nitrosothiols (Table 3) as well as of the nitrosothiols protonated at the N atom (Table 4): in all cases the LUMO orbital is spread almost uniformly over the S, N and O atoms and has symmetry appropriate to overlap with the thiolate HOMO (Fig. 6).

Table 2 Charges at the S atom and characteristics of frontier orbitals of the studied thiolates, RS^{n-}

Thiolate	q_T[a]	q_S	E_{HOMO}/eV % AO's in MO	E_{LUMO}/eV % GO's[b] in MO	ΔE[c] /eV
N-Acetylcysteine	−2	−0.69	+3.73 88 S	+6.92 79 C_2H_5COO	3.19
Ethyl cysteinate	−1	−0.56	+0.69 91 S	+2.49 83 COO	1.80
Cysteine	−2	−0.75	+4.70 91 S	+8.89 67 COO	4.19
Glutathione	−3	−0.61	+4.54 91 S	+7.66 75 CONH	3.12

[a] Total charge of the entity. [b] Group orbitals. [c] HOMO-LUMO energy gap.

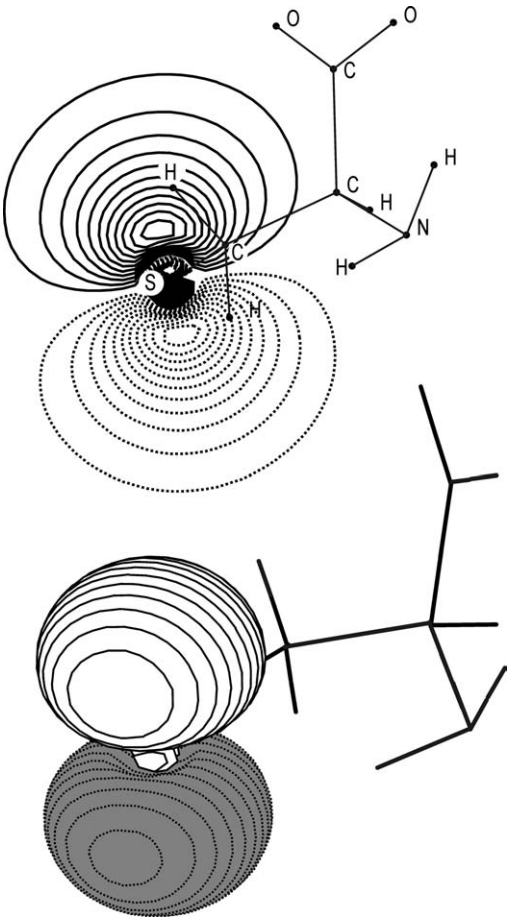

Fig. 5 HOMO orbital for the cysteine molecule; contour (cut through the plane containing S and C_1 atoms) and orbital plots.

The ligand that is present in the transient $[Fe(CN)_5N(O)(SR)_2]^{(2n+2)-}$ complex resembles the thiol-nitrosothiol adduct, $(RS)_2NOH$, and similarly may undergo homolytic and heterolytic splittings of the S–N bond.[43–52] The successive processes are not obvious, but the electron transfer towards the $[Fe(CN)_5]$ moiety could be facilitated by the positive charge on the sulfur atom of $RSNO^{(n-1)-}$ ($q \sim +0.3$, *cf.* Table 3). The sulfur charge is considerably increased (up to $q \sim +0.5$) when the electron density on the N atom is decreased by proton association (Table 4). This tendency should be even intensified by the coordination of the $RSNO^{(n-1)-}$ ligand to the Fe centre.

Concluding remarks

The analysis of the thermal reactivity of the $[Fe(CN)_5N(O)SR]^{(n+2)-}$ complexes (where H_nRS = cysteine, *N*-acetylcysteine, ethyl cysteinate and glutathione) reveals their very complicated behaviour. The redox decomposition occurs *via* spontaneous homolytic splitting [eqn. (3)] and autocatalysed redox processes [eqns. (6)–(9)], in which the $RS^{\bullet(n-1)-}$ and $RSSR^{\bullet(2n-1)-}$ radicals play a crucial role. The chain termination consists in scavenging the $RSSR^{\bullet(2n-1)-}$ radicals by nitroprusside, accompanied with generation of the final products, $[Fe(CN)_5NO]^{3-}$ and disulfide [eqn. (9)]. The processes are preceded by a pre-equilibrium [eqn. (1)] and kinetic traces show an induction period, followed by pseudo-zero-order and pseudo-first-order segments. The proposed mechanism is supported by DFT calculations (Tables 2–4, Figs. 5 and 6). The results provide an understanding of the particular steps of both pathways of the redox decomposition. The results of the calculations justify also the propensity of nitrosothiols and nitrosothiolates to react with thiols and thiolates, respectively.

In reality, however, the studied systems are even much more complicated than it is shown in this paper. First, the thiols, both free and bonded as ligand, are involved in the protonation equilibria, which were not taken into consideration. Second, cyanometallates are known for their tendency to form ion pairs,[16,17] and a similar behaviour is expected also for all the complexes, as well as thiolates, present in the studied systems. Moreover, rate constants for different redox reactions involving cyanometallates strongly depend on the concentration and type of cations.[69–72] Thus, the additional equilibria, including ion-pair formation, should be taken into account in more sophisticated kinetic studies. To get the essential data, experimental work on ion-pair formation in the $[Fe(CN)_5NO]^{2-}$-thiolate system is reported elsewhere.[72]

Experimental

Chemicals

Sodium nitroprusside (Merck), glutathione (Aldrich), *N*-acetylcysteine (Merck), cysteine hydrochloride (Aldrich) and ethyl cysteinate hydrochloride (Aldrich) of highest available purity were used as purchased. All measurements were performed at 298 K, in buffered solutions (pH 10), containing 0.25 M Na_2CO_3, 0.082 M $Na_2B_4O_7$ and 0.001 M Na_2edta, with total sodium concentration of 0.666 M. The reagent concentrations used in kinetic measurements were as follows: 1 mM thiolate with 0.01–0.2 M nitroprusside (in the case of nitroprusside excess), and 1 mM nitroprusside with 0.01–0.2 M thiolate (at thiolate excess).

Instrumentation

UV-Vis spectra were measured in quartz tandem cells of 0.864 cm pathlength on Shimadzu UVPC 2001 and HP8453 spectrophotometers. Slow kinetic traces (nitroprusside in excess) were recorded on a Shimadzu UVPC 2001 spectrophotometer whereas a SX17MV stopped flow apparatus (Applied

Table 3 Atomic charges and characteristics of frontier orbitals of *S*-nitrosothiols, $RSNO^{(n-1)-}$, derived from the studied thiolates

Thiolate	q_T[a]	q_S	q_N	q_O	E_{HOMO}/eV % GO's[b] in MO	E_{LUMO}/eV % AO's in MO	ΔE[c]
N-Acetylcysteine	−1	+0.30	−0.14	−0.23	−1.29 79 COO	−0.27 19 S, 47 N, 31 O	1.02
Ethyl cysteinate	0	+0.28	−0.08	−0.15	−5.92 72 NH_2 10 COO	−4.12 15 S, 50 N, 32 O	1.80
Cysteine	−1	+0.30	−0.18	−0.23	−0.64 81 COO	−0.12 17 S, 45 N, 30 O	0.52
Glutathione	−2	+0.32	−0.18	−0.20	+1.00 75 COO 15 NH_2	+1.02 16 S, 47 N, 31 O	0.02

[a] Total charge of the entity. [b] Group orbitals. [c] HOMO-LUMO energy gap.

Table 4 Atomic charges and characteristics of frontier orbitals of *N*-protonated *S*-nitrosothiols, $RSNOH^{(n-2)-}$, derived from the studied thiolates

Thiolate	q_T[a]	q_S	q_N	q_O	q_H	E_{HOMO}/eV % GO's[b] in MO	E_{LUMO}/eV % AO's in MO	ΔE[c]
N-Acetylcysteine	0	+0.53	−0.26	−0.20	+0.43	−5.89 79 COO	−5.69 18 S, 30 N, 30 O	0.20
Ethyl cysteinate	+1	+0.53	−0.22	−0.12	+0.48	−10.36 57 NH_2 22 COO	−10.18 19 S, 35 N, 33 O	0.18
Cysteine	0	+0.50	−0.29	−0.19	+0.42	−5.73 91 COO	−5.69 15 S, 28 N, 30 O	0.04
Glutathione	−1	+0.45	−0.28	−0.20	+0.40	−2.83 57 COO 20 NH_2	−2.82 12 S, 28 N, 30 O	0.01

[a] Total charge of the entity. [b] Group orbitals. [c] HOMO-LUMO energy gap.

Photophysics) was used in the case of the thiolate excess. All kinetic measurements were performed under pseudo-first-order conditions. Room temperature ESR measurements were made on a Bruker EMS spectrometer operating at the X band with 100 kHz modulation in flat quartz cells with DPPH as internal standard. Electrochemical experiments were carried out by use of CV50W (Bioanalytical Systems) and CX-741 (Elmetron) electrochemical analysers. For spectroelectrochemical monitoring of $[Fe(CN)_5NO]^{2-}$ reduction, a 2 mm quartz cell was equipped with a Pt–Ir minigrid electrode (5% Ir), auxiliary electrode (Pt wire) and reference Ag/AgCl electrode (FLEX-REF, World Precision Instruments). Oxygen concentration was measured using a CTN-920.S electrochemical sensor with PTFE membrane (Elsent, Poland).

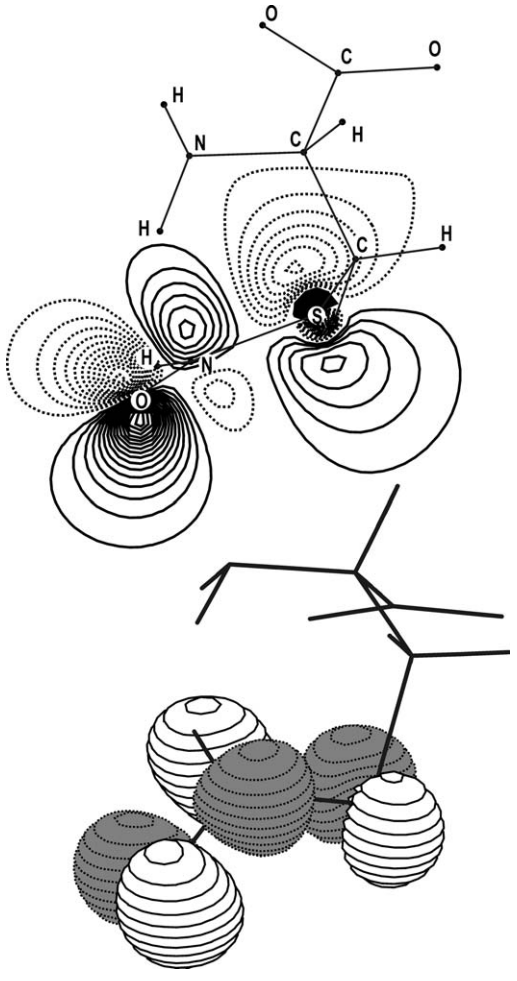

Fig. 6 LUMO orbital for the *N*-protonated *S*-nitrosocysteine molecule; contour (cut through the plane containing O and S atoms) and orbital plots.

Calculations and modelling

Kinetic traces of the $[Fe(CN)_5N(O)SR]^{(n+2)-}$ decay were processed using standard stopped flow kinetic software supplied by Applied Photophysics and Gepasi (version 3.21).[73–75] Pseudo-first-order rate constants for spontaneous decomposition of the complex [eqn. (3)] were calculated from mono-exponential fits to experimental kinetic traces. k_{obs} values were found to be concentration independent. In the case of thiol excess, pseudo-zero-order rate constants (k_0) were calculated from the slopes of the linear segment of the kinetic traces at high thiolate excess, whereas pseudo-first-order rate constants were determined from mono-exponential fits at lower thiolate concentration. Concentration dependence of the k_{obs} values allowed for the k_I determination [eqn. (12) or (13)].

DFT calculations[66] were made using the DFT-LCGTO program package.[76] For the exchange and correlation, the local-density approximation (DFT-LDA) with the Vosko–Wilk–Nusair (VWN) parameterisation[77] was used. Kohn–Sham orbitals were represented by linear combinations of atomic orbitals using extended basis sets of contracted Gaussian-type orbitals (CGTO) of double zeta quality. Traditional quantum mechanical tools such as Mulliken population analysis,[78] electron density plots of the frontier orbitals as well as characterisation of HOMO and LUMO orbitals was applied to examine inter-atomic binding.

Acknowledgements

The authors thank Professor Orazio Traverso (University of Ferrara), Professor Rudi van Eldik (University of Erlangen-Nürnberg) and Professor Marcel Maeder (University of Newcastle, Australia) for valuable discussions.

References

1 J. S. Stamler, D. J. Singel and J. Loscalzo, *Science*, 1992, **258**, 1898.
2 J. S. Stamler, *Cell*, 1994, **78**, 931.
3 L. J. Ingarro, *Angew. Chem. Int. Ed. Engl.*, 1999, **38**, 1882.
4 I. L. Megson, *Drugs Future*, 2000, **25**, 701.
5 J. Stamler and A. Hausladen, *Nat. Struct. Biol.*, 1998, **5**, 247.
6 G. Stochel, M. Pawelec and Z. Stasicka, *Wiad. Chem.*, 1997, **51**, 163.
7 M.-C. Broillet, *Cell. Mol. Life Sci.*, 1999, **55**, 1036.
8 D. R. Adams, M. Brochwicz-Lewinski and A. R. Butler, *Prog. Chem. Org. Nat. Prod.*, 1999, **76**, 1.
9 F. Murad, *Angew. Chem., Int. Ed.*, 1999, **38**, 1856.
10 R. F. Furchgott, *Angew. Chem., Int. Ed.*, 1999, **38**, 1870.
11 Z. Guo and P. J. Sadler, *Adv. Inorg. Chem.*, 2000, **49**, 183.
12 A. R. Butler and I. L. Megson, *Chem. Rev.*, 2002, **102**, 1155.
13 P. G. Wang, M. Xian, X. Tang, X. Wu, Z. Wen, T. Cai and A. J. Janczuk, *Chem. Rev.*, 2002, **102**, 1091.
14 M. D. Johnson and R. G. Wilkins, *Inorg. Chem.*, 1984, **23**, 231.
15 A. R. Butler and C. Glidewell, *Chem. Soc. Rev.*, 1987, **16**, 361.

16 K. Szaciłowski, G. Stochel, Z. Stasicka and H. Kisch, *New J. Chem.*, 1997, **21**, 893.
17 O. R. Leeuwenkamp, C. H. Vermaat, C. M. Plug and A. Bult, *Pharm. Weekbl. [Sci. Ed.]*, 1984, **6**, 195.
18 A. R. Butler, A. M. Calsy-Harrison, C. Glidewell and P. E. Sørensen, *Polyhedron*, 1988, **7**, 1197.
19 A. R. Butler, A. M. Calsy-Harrison, C. Glidewell, I. L. Johnson, J. Reglinski and W. E. Smith, *Inorg. Chim. Acta*, 1988, **151**, 281.
20 A. R. Butler, A. M. Calsy and I. L. Johnson, *Polyhedron*, 1990, **9**, 913.
21 P. J. Morand, E. B. Borghi, L. M. de Schteingart and M. A. Blesa, *J. Chem. Soc., Dalton Trans*, 1981, 435.
22 D. Mulvey and W. A. Waters, *J. Chem. Soc., Dalton Trans.*, 1975, 951.
23 K. Antal, I. Bányai and M. Beck, *J. Chem. Soc., Dalton Trans.*, 1985, 1191.
24 A. Kovács and I. Bányai, *J. Inorg. Biochem.*, 1995, **59**, 191.
25 D. Tsikas, R. H. Böger, S. M. Bode-Böger, G. Brunner and J. Frölich, *J. Chromatogr. A*, 1995, **699**, 363.
26 J. Reglinski, A. R. Butler and C. Glidewell, *Appl. Organomet. Chem.*, 1994, **8**, 25.
27 S. Aleryani, E. Milo and P. Kostka, *Biochim. Biophys. Acta*, 1999, **1472**, 181.
28 K. Szaciłowski, J. Oszajca, A. Barbieri, A. Karocki, Z. Sojka, S. Sostero, R. Boaretto and Z. Stasicka, *J. Photochem. Photobiol. A: Chem.*, 2001, **143**, 99.
29 R. P. Cheney, M. G. Simic, M. Z. Hoffman, I. A. Taub and K.-D. Asmus, *Inorg. Chem.*, 1977, **16**, 9.
30 J. Fiedler, *Collect. Czech. Chem. Commun.*, 1993, **58**, 461.
31 H. M. Carapuça, J. E. J. Simão and A. G. Fogg, *Port. Electrochim. Acta*, 1995, **13**, 349.
32 J. D. W. van Voorst and P. Hemmerich, *J. Chem. Phys.*, 1966, **45**, 3914.
33 A. Wanat, R. van Eldik and G. Stochel, *J. Chem. Soc. Dalton Trans.*, 1998, 2497.
34 J. Schmidt, H. Kühr, W. L. Dorn and J. Kopf, *Inorg. Nucl. Chem. Lett.*, 1974, **10**, 55.
35 H. M. Carapuça, J. E. J. Simão and A. G. Fogg, *Analyst*, 1996, **121**, 1801.
36 H. M. Carapuça, J. E. J. Simão and A. G. Fogg, *J. Electroanal. Chem.*, 1998, **455**, 93.
37 J. D. Schwane and M. T. Ashby, *J. Am. Chem. Soc.*, 2002, **124**, 6822.
38 C. Terille, O. R. Nascimento, I. J. Moraes, E. E. Castellano, O. E. Piro, J. A. Güida and P. J. Aymonino, *Solid State Commun.*, 1990, **73**, 481.
39 D. E. Wilcox, H. Kruszyna, R. Kruszyna and R. P. Smith, *Chem. Res. Toxicol.*, 1990, **3**, 71.
40 B. A. Goodman and J. B. Raynor, *J. Chem. Soc. A*, 1970, 2038.
41 M. C. R. Symons, J. G. Wilkinson and D. X. West, *J. Chem. Soc., Dalton Trans.*, 1982, 2041.
42 R. G. Wilkins, *Kinetics and Mechanism of Transition Metal Complexes*, VCH, Weinheim, Cambridge, 1991.
43 K. Szaciłowski and Z. Stasicka, *Prog. React. Kinet. Mech.*, 2000, **26**, 1.
44 S. P. Mezyk and D. A. Armstrong, *J. Chem. Soc., Perkin Trans. 2*, 1999, 1411.
45 S. Charles, J. P. Lecomte, C. Desfrançois, S. Xu, J. M. Nilles, K. H. Bowen, J. Bergès and C. Hourèe-Levin, *J. Phys. Chem. A*, 2001, **105**, 5622.
46 R. Benassi and F. Taddei, *J. Phys. Chem. A*, 1998, **102**, 6173.
47 S. P. Mezyk, *Chem. Phys. Lett.*, 1995, **235**, 89.
48 S. P. Mezyk, *J. Phys. Chem.*, 1996, **100**, 89.
49 M. G. Bonini and O. Augusto, *J. Biol. Chem.*, 2001, **276**, 9749.
50 M. Quintiliani, R. Badiello, M. Tamba, A. Estefandi and G. Gorin, *Int. J. Radiat. Biol.*, 1977, **32**, 195.
51 J. P. Barton and J. E. Packer, *Int. J. Radiat. Phys. Chem.*, 1970, **2**, 159.
52 R. Zhao, J. Lind, G. Merényi and T. Eriksen, *J. Am. Chem. Soc.*, 1994, **116**, 12 010.
53 D. R. Arnelle, B. J. Day and J. S. Stamler, *Nitric Oxide*, 1997, **1**, 56.
54 K. Wang, W. Zhang, M. Xian, Y.-C. Hou, X.-C. Chen, J.-P. Cheng and P. G. Wang, *Curr. Med. Chem.*, 2000, **7**, 821.
55 D. L. H. Williams, *Acc. Chem. Res.*, 1999, **32**, 869.
56 T. Komiyama and K. Fujimori, *Bioorg. Med. Chem. Lett.*, 1997, **7**, 175.
57 S. P. Singh, J. S. Wishnok, M. Keshive, W. M. Deen and S. R. Tannenbaum, *Proc. Natl. Acad. Sci. USA*, 1996, **93**, 14 428.
58 K. Wang, Z. Wen, W. Zhang, M. Xian, J.-P. Cheng and P. G. Wang, *Bioorg. Med. Chem. Lett.*, 2001, **11**, 433.
59 A. P. Dicks, E. Li, A. P. Munro, H. R. Swift and D. L. H. Williams, *Can. J. Chem.*, 1998, **76**, 789.
60 P. S.-Y. Wong, J. Hyun, J. M. Fukuto, F. G. Shirota, E. D. DeMaster, D. W. Shoeman and H. T. Nagasawa, *Biochemistry*, 1998, **37**, 5362.
61 H. Karoui, N. Hogg, C. Fréjaville, P. Tordo and B. Kalyanaraman, *J. Biol. Chem.*, 1996, **271**, 6000.
62 R. Zhao, J. Lind, G. Merényi and T. E. Erikson, *J. Chem. Soc., Perkin Trans. 2*, 1997, 569.
63 M. Jonsson and H.-B. Kraatz, *J. Chem. Soc., Perkin Trans. 2*, 1997, 2673.
64 A. Del Corso, P. G. Vilardo, M. Capiello, I. Cecconi, M. Dal Monte, D. Barsachi and U. Mura, *Arch. Biochem. Biophys.*, 2002, **397**, 392.
65 Y. Chen and W. Maret, *Eur. J. Biochem.*, 2001, **268**, 3346.
66 R. G. Parr, and W. Yang, *Density Functional Theory of Atoms and Molecules*, Oxford University Press, Oxford, 1989.
67 R. G. Pearson, *J. Chem. Educ.*, 1987, **64**, 561.
68 R. G. Pearson, *Inorg. Chem.*, 1988, **27**, 734.
69 P. D. Metelski and T. W. Swaddle, *Inorg. Chem.*, 1999, **38**, 301.
70 Y. Fu and T. W. Swaddle, *Inorg. Chem.*, 1999, **38**, 876.
71 A. Zahl, R. van Eldik and T. W. Swaddle, *Inorg. Chem.*, 2002, **41**, 757.
72 G. A. Lawrance, M. Maeder, B. Neuhold, K. Szaciłowski, A. Barbieri and Z. Stasicka, *J. Chem. Soc., Dalton Trans.*, 2002, in press (DOI: 10.1039/b205536h).
73 P. Mendes, *Comput. Appl. Biosci.*, 1993, **9**, 563.
74 P. Mendes, *Trends Biochem. Sci.*, 1997, **22**, 361.
75 P. Mendes and D. B. Kell, *Bioinformatics*, 1998, **14**, 869.
76 DFT-LCGTO programme package named StoBe developed by A.S.T.-Amant and D. Salahub (Canada) and elaborated by L. Pettersson (Sweden) and K. Hermann (Germany) (non commercial).
77 S. H. Vosko, L. Wilk and M. Nusair, *Can. J. Phys.*, 1980, **58**, 1200.
78 R. S. Mulliken, *J. Chem. Phys.*, 1955, **23**, 2388.